JOURNAL OF PROPULSION AND POWER
Vol. 25, No. 2, March–April 2009

Experimental Investigation of Thermoacoustic Coupling for Low-Swirl Lean Premixed Flames

Yun Huang* and Albert Ratner†
University of Iowa, Iowa City, Iowa 52242

DOI: 10.2514/1.36310

Combustion instabilities are frequently encountered in gas turbine engines. The main physical mechanism that leads to combustion instability is thermoacoustic coupling, where energy released as part of the combustion process is transferred into combustor acoustics, which can then affect the combustion heat release in a feedback process. This paper presents an experimental study of this coupling for a lean premixed methane–air low-swirl flame. Planar laser-induced fluorescence of the hydroxyl radical was employed to measure the behavior of this flame in an acoustically driven environment and the Rayleigh index was used as an indicator of the thermoacoustic coupling. The acoustic excitation ranged from 13 to 270 Hz. Experiments show that the coupling occurred within certain frequency subranges depending on the Reynolds and Strouhal number. The acoustic excitation can couple with the shear-layer vortices, which in turn wrinkle the flame with a periodicity similar to the acoustic driving. This effect, through the changes in local flame surface density, gives rise to intense toroidal structures in the Rayleigh index field.

I. Introduction

COMBUSTION efficiency improvements and pollutant emission reduction have become ever-increasing issues of global concern. For many combustion systems, a lean premixed combustion scheme can increase the fuel efficiency and reduce the emission of NO_x. However, as the fuel–air mixture in the system becomes progressively lean, the system becomes susceptible to perturbations which can change the unsteady heat release pattern and lead to combustion instability [1,2]. The combination of this problem with the general problem of stabilizing premixed flames has been a key issue for modern combustion technology; yet this problem is far from being well understood for complex combustion systems. One new burner design that seems to meet many of the desired criteria is the low-swirl burner developed by R. K. Cheng et al. [3]. The low-swirl burner (LSB) has been shown to reduce pollutant emission and has a wider operating range than currently employed high-swirl industrial burners. This paper presents an experimental study performed on the low-swirl-stabilized, lean premixed methane–air flame generated with this burner with the focus of the investigation being thermoacoustic coupling.

Extensive research has been carried out to examine both devices and technical issues to aid in the understanding, prediction, and control of combustion instability [4]. Many factors have been identified as pertinent to combustion instability, including the equivalence ratio, flowfield, background noise, temperature of the reactants, etc. Particularly, it has been shown that small variations in equivalence ratio can lead to large fluctuations in heat release, especially when the mixture fraction approaches the lean limit, with any factor that affects the mixing being capable of inducing instability [5–8]. The flowfield affects the combustion instability in many ways. Mixing layers play a dominant role for diffusion combustion. For premixed combustion, the vortices can not only distort the flame front and cause flame stretch, but the vortex shedding can generate noise and interact with the combustion process [9–14]. The interaction between a vortex and a flame and the interaction between an acoustic wave and a flame front have been the focus of concerted research and examined on different types of combustors. Ghoniem et al. conducted research on a dump combustor and observed that an unstable shear layer acted as the source of sustained oscillations [10]. Matveev and Culick derived a reduced-order model for interaction among vortex shedding, chamber acoustics, and combustion in a dump combustor [11]. Birbaud et al. studied acoustic response of a laminar premixed conical flame and observed different coupling mechanisms at low and high frequencies [13]. Huang et al. studied combustion dynamics in a lean, premixed swirl-stabilized combustor with numerical simulation and showed that the inlet temperature and equivalence ratio are the key parameters determining the stability characteristic [14]. These are but a few examples out of a large amount of pertinent literature. Unfortunately, even with the significant work to date, there is still no consensus on the interaction of the physical mechanisms that result in combustion instability.

In studying these mechanisms, one of the primary methods has been to drive the system with acoustic excitation. Techniques include varying the chamber geometry to induce natural acoustic oscillations [12] and acoustic driving of the incoming reactants/fuel supply [9,13,15,16]. The work described here (and related work carried out previously by Kang et al. [17]) is based on placing the flame in an acoustic chamber and driving the field from the downstream direction. Each of the methods has particular advantages and disadvantages. Naturally (acoustically) active systems are extremely dependent on geometry, and are primarily used for examination of combustor geometry rather than assessment of particular burner characteristics. Inducing acoustics/flame oscillation by perturbing the reactant supply (usually with a speaker) requires perturbation at 5–15% of the bulk flow, according to most reports. For example, the work of Balachandran et al. [18] shows oscillatory driving with a velocity amplitude of 15% of the bulk velocity, and work by Birbaud et al. [13,15] has an oscillatory velocity amplitude of more than 7% of the mean flow. This level of driving creates similar oscillations in the mass flow at the burner exit and creates strong vorticity at the burner edge. Although in some real circumstances the combustion oscillations were caused by large amplitude oscillation in the fuel supply system, the results from this type of research have been industrially applied and current designs have significantly improved fuel system performance. The current work is different from the aforementioned because the acoustic driving comes from downstream and is approximately 0.1% of chamber pressure. The objective of the work is, then, also very different, in that it studies how weak forcing, typical of ambient conditions, leads to coupling and growth of unstable modes.

Received 21 December 2007; revision received 3 July 2008; accepted for publication 20 October 2008.

*Ph.D. Student, Department of Mechanical and Industrial Engineering; yun-huang@uiowa.edu. Student Member AIAA.

†Assistant Professor, Department of Mechanical and Industrial Engineering; albert-ratner@uiowa.edu. Senior Member AIAA.

This work continues and expands on the study of Kang et al. [17] by further investigating how extremely weak forcing can induce significant flowfield and flame changes. In that work, OH planar laser-induced fluorescence was used to measure OH concentration changes for an acoustically perturbed, lean premixed methane–air flame. Toroidal structures in the Rayleigh index were detected along the shear layer for a range of equivalence ratios and driving frequencies. The equivalence ratio (with tested values of 0.5, 0.6, and 0.75) was found to have little effect on the structure of the Rayleigh index, whereas the excitation frequency produced significantly different structures. In this study, similar experiments are conducted on the same burner, but with a different chamber, fuel supply system, and chamber acoustic boundaries. This allows an assessment of burner behavior, as opposed to chamber or fuel supply issues. In addition, analysis of local flame/flow interaction is provided to give new insight into how this phenomenon occurs.

Examination of thermoacoustic coupling requires a reliable indicator of heat release rate and an indicator that is capable of resolving spatial structures in turbulent flames [19]. The hydroxyl radical (OH) is an important participant in the flame front combustion reactions that exist in significant concentrations. Conversely, it has a relatively long lifetime and is present as an equilibrium product in the hot, burnt gas region. This aspect would disqualify it except that it has been shown that OH concentrations in the flame front of lean and stoichiometric methane–air flat flames is much higher than that found in burnt gas regions [20,21]. Estimates of the flame area from OH planar laser-induced fluorescence (PLIF) were shown sufficient to determine heat release rate for perturbations less than 15% of the bulk velocity [18]. At the end of this paper, the flame surface density is shown to closely follow the OH intensity.

II. Experimental Setup

The experimental facility used in this study comprises an acoustic chamber, a swirl burner, a fuel premixer, and a PLIF measurement system. A schematic illustration of the chamber and burner is shown in Fig. 1. The stainless steel chamber is made of a vertical central section and a horizontal top that houses the loudspeakers. The inside diameter of the combustion chamber is about 30 cm and the height is approximately 185 cm. The bottom part of the chamber is equipped with quartz windows to provide full optical access to the flame. The top of the chamber in this work is equipped with adjustable valves which create an acoustically closed exit condition and enables pressurized experimentation. The first mode of the resonance frequency is 82 Hz if the major component of gas in the chamber is nitrogen at 300 K. This frequency will shift to 88 Hz if the mean temperature rises to 350 K.

The low-swirl burner in this work is the kind of burner developed in Cheng et al. [3]. The low-swirl burner stabilizes flame by flow divergence rather than with a central recirculation zone as is characteristic of high-swirl burners. The inside diameter of the burner is 2.54 cm and the swirl number is approximately 0.5. The burner is located at the bottom of the chamber and is supplied with a fully premixed methane/air mixture from a custom-designed mixer. The mixer is 4.8 cm in diameter, 20 cm long, and it has 14 disks inside for complete mixing. The burner in this work is operated at lean conditions. The mass flow rates, the equivalence ratio, and the corresponding Reynolds numbers are listed in Table 1.

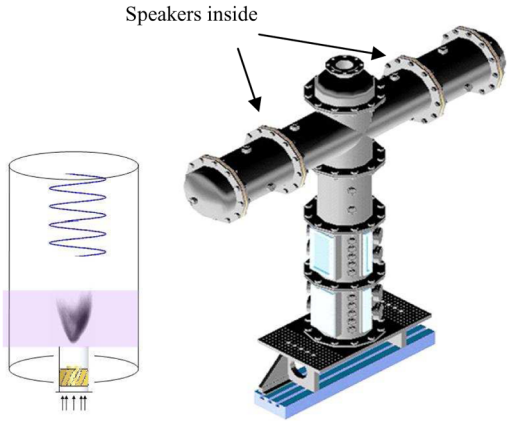

Fig. 1 Schematic views of the acoustic chamber and swirl burner.

Table 1 Experimental conditions

	Φ	$\dot{m}_{\text{air}}$	$\dot{m}_{\text{CH4}}$	Re
Case 1	0.50	2.16	0.06	5865
Case 2	0.59	3.13	0.11	8547

The speakers in the upper part of the chamber provide acoustic perturbations at desired frequencies. The acoustic signal is detected by a high resolution piezoelectric pressure transducer and then actively controlled to ensure that only the intended driving mode is present and that the wave amplitude is at the preselected level [17]. The length scale of the flame is much smaller than that of the driven acoustic wavelength, ensuring that the pressure oscillation is approximately constant (spatially) across the whole flame. For example, at room temperature, the wavelength of 200 Hz excitation is approximately 1.7 m. The flame region we observe is about 7 cm high and is at the bottom of the chamber, which is a pressure node. The spatial span corresponds to less than 15 deg of variance (out of 360 deg for the full acoustic wave), which means an amplitude change of less than 5%. For lower frequencies, the difference is even less.

The laser system consists of a pump laser, a dye laser, and an optical frequency doubler. The Nd:YAG pump laser optically drives the dye laser, whose output is then doubled to provide the requisite UV radiation for excitation of the fluorescence of OH radical. The power of the final UV beam for fluorescence is approximately 25 mJ/pulse. The dye laser is tuned so that the final beam is at the selected rovibronic transitions of OH in the $A \leftarrow X(1,0)$ band. The fluorescence from planar laser-induced fluorescence of the hydroxyl radical (OH-PLIF) is collected at 90 deg from the laser sheet with a 105 mm f/1.2 UV lens attached to an intensified charged-coupled device (ICCD) camera. The image field is approximately 10 cm square and the resolution is set at 512×512 pixels. The electronic image intensifier for the camera is triggered synchronously with the laser pulse. A band pass filter (312.6F10-10) is installed in the ICCD camera to cut off all scattered light and to pass only the OH fluorescence in the 300–320 nm range. For each frequency, three sets of 300 images (3×300) were collected.

III. Results and Discussion

In the current experimental setup, no self-induced strong acoustics have ever been detected. The lack of a self-induced oscillation may be attributed to a relatively big chamber (having significant area for dissipation) or inhabitation by flame geometry. As is known for thermoacoustic engines where oscillations are desired, there must be enough of a temperature gradient and appropriate geometry to excite resonance [22]. Here, the combustion process (most likely) does not release enough energy to create a large enough temperature gradient across a short distance in the chamber. In addition, the burner is not at the quarter-wave position to trigger the thermoacoustic oscillation. Naturally induced oscillations are often observed in dump combustors or confined geometries [5,12]. Figure 2 compares the pressure oscillations under different conditions. Figure 2a was taken without acoustic driving, Fig. 2b is at 45 Hz excitation, and Fig. 2c is at 85 Hz excitation. Figure 2d is taken under cold-flow conditions and 45 Hz excitation. Compared with flame condition, there is more high-frequency noise in the cold-flow case, possibly due to the filtering effect of flame dilatation [23].

Figure 3 compares the low-swirl-stabilized, lean premixed methane–air flame at different conditions. The images are of the instantaneous Fig. 3a and mean Fig. 3b OH intensity. The left image

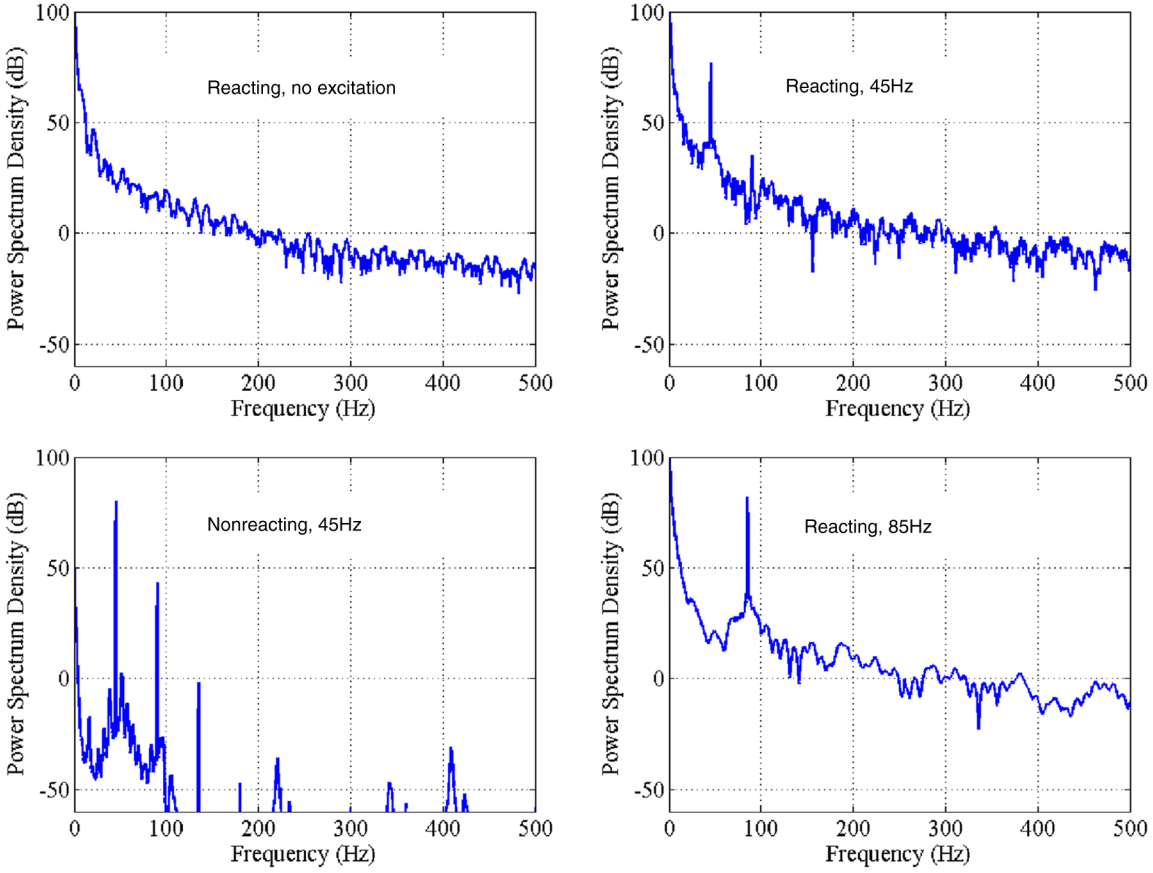

Fig. 2 Power spectrum density of the pressure oscillations.

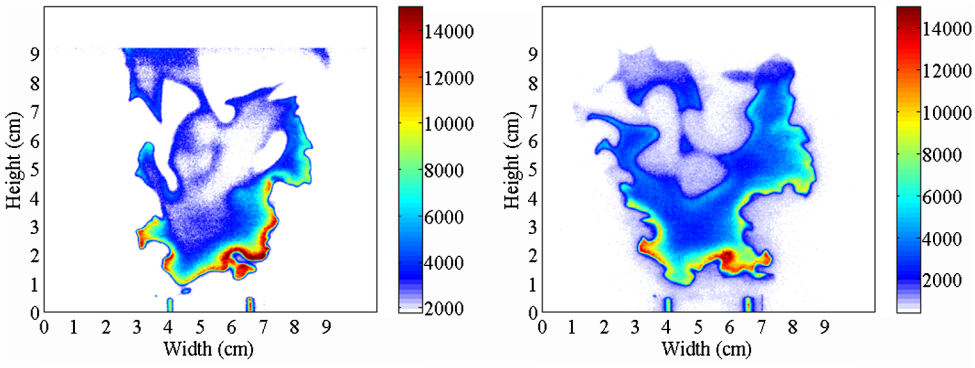

a) Instantaneous PLIF images of the LSB flame (left, no excitation; right, 100Hz (0.09%))

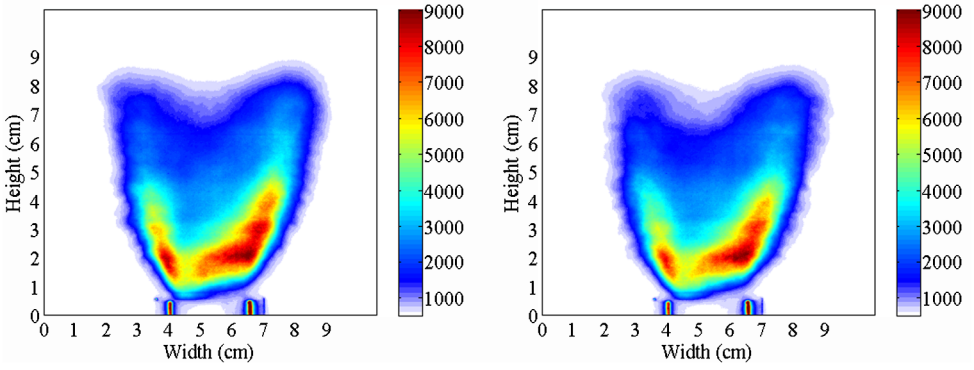

b) Mean PLIF images of the LSB flame (left, no excitation; right, 100Hz (0.09%))

Fig. 3 PLIF images of the LSB flame [left, no excitation; right, 100 Hz (0.09%)]: a) instantaneous, b) mean.

in each set is taken without acoustic excitation and the right image is with 100 Hz excitation where the pressure oscillation amplitude is 0.09%. This oscillation amplitude is typical for all of the experiments described herein. Such small amplitude acoustic forcing assures an acoustical velocity fluctuation which is smaller than the turbulence level. For a typical acoustic wave, the induced velocity [7] is $u'_a \sim p'(\bar{\rho}c)^{-1} = 0.2$ m/s for a driving pressure of 90 Pa. The turbulence level of the low-swirl flow is generally about 0.1% of the mean flow [3], $u' \sim 0.1 \times u = 0.5$ m/s. The image pairs (both instantaneous and averaged) show little difference, as would be expected due to the low driving amplitude and the strong flame turbulence.

A. Rayleigh Index Distribution

The Rayleigh index has been considered an important indicator of thermoacoustic coupling in many research studies [6]. If the Rayleigh index is positive, pressure oscillation and heat release oscillation are coupled and tend to grow. If the Rayleigh index is negative, the oscillation tends to decay. In this study, this index is examined as a major system parameter. The simplified normalized Rayleigh index is defined as

$$R_f = \int_0^1 \frac{p'q'}{p_{\text{rms}}\bar{q}}\,\mathrm{d}\xi$$

where p' is the pressure oscillation, p_{rms} is the root mean square of the pressure oscillation for each set of images, q' is the oscillation of the OH intensity (heat release) of each pixel, and $\bar{q}$ is the averaged total OH intensity. Clearly distinguishable structures were observed in the Rayleigh index distribution, although few differences were observable in the OH images. Figure 4 shows a typical set of Rayleigh index distributions with acoustic excitation frequencies ranging from 13 to 208 Hz. The mean velocity at the burner exit is 3.48 m/s and the equivalence ratio is 0.5. The Rayleigh index appears to show cross sections of a series of toroidal structures in 3-D. Although these positive (unstable) or negative (stable) structures are seen in the local Rayleigh index distribution, the global Rayleigh indexes (Fig. 5) are close to zero, despite the different spatial distributions (global means the whole image region). The preceding phenomena appear to be similar to the work of Kang et al. [17], but here the chamber geometry, the fuel premixer, and the mass flow rates are all quite different. This suggests that the coupling behavior and the resulting toroidal structure in Rayleigh index maps are characteristics of the low-swirl burner and are not related to the rest of the combustion system.

In the current configuration, the premixed reactants pass through the swirler inside the burner and then exit the burner as a freejet; above the burner (postcombustion) are hot products surrounded by nitrogen coflow. The natural buoyancy of the flame interacts with the

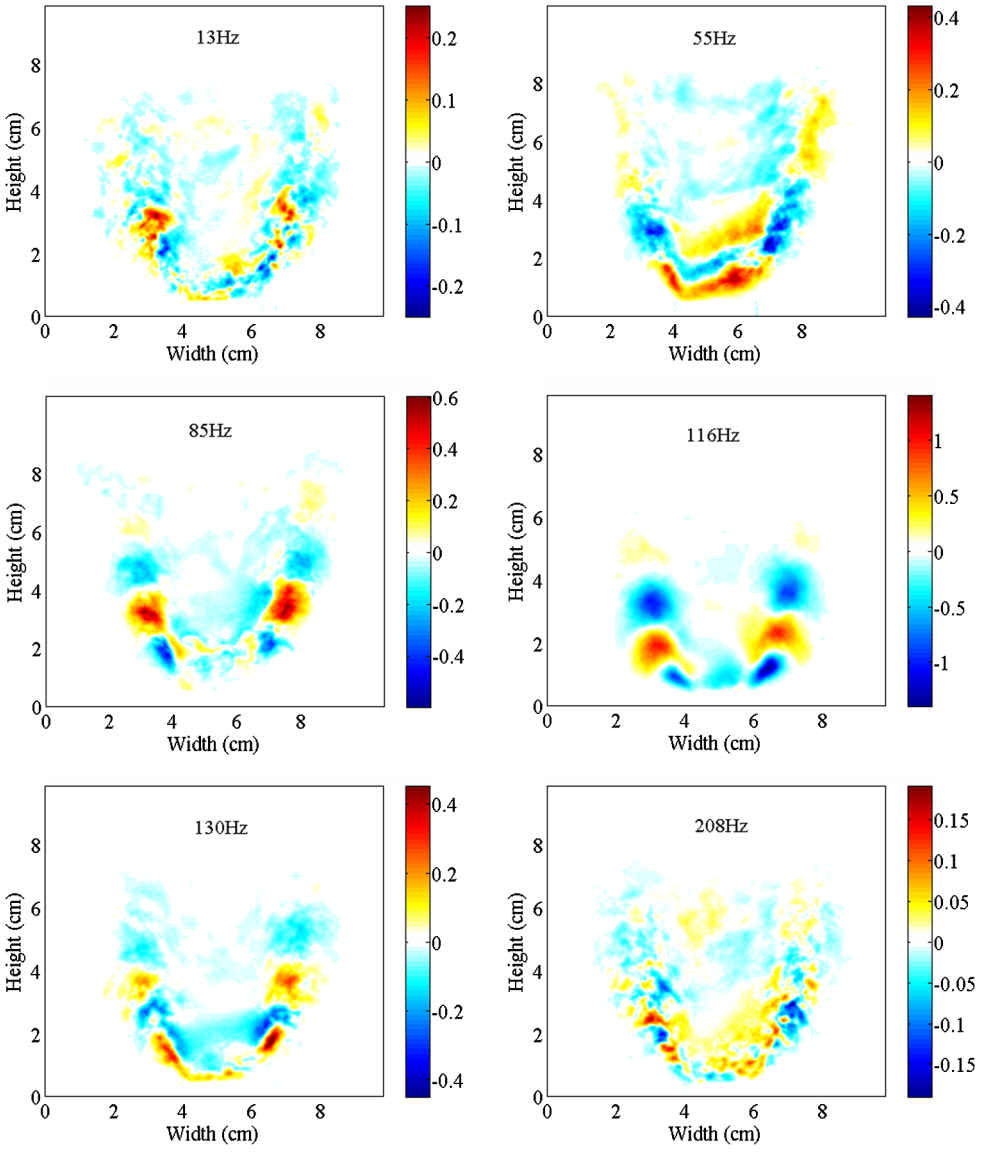

Fig. 4 Rayleigh index of the cross section of the flame with enforced acoustics ($P = 1$ atm, $\Phi = 0.5$, $f = 13, 55, 85, 116, 130, 208$ Hz).

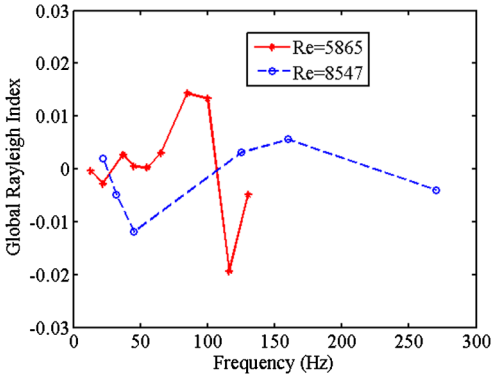

Fig. 5 Global Rayleigh index.

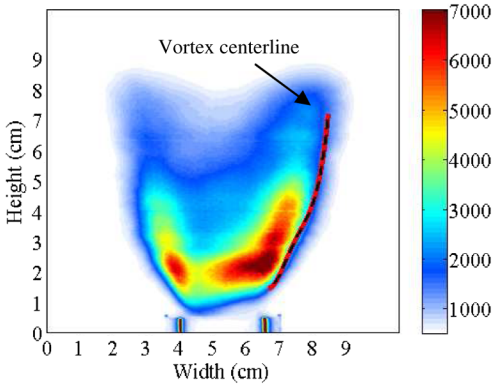

Fig. 6 Vortex centerline ($f = 85$ Hz, $Re = 5865$, $\Phi = 0.51$).

low-swirl jet and creates a modified buoyant jet-type flowfield. The flowfield for the burner has been previously measured through particle imaging velocimetry (PIV) by Littlejohn and Cheng [24], and their results are applied here to extract the approximate flowpath of interest. Figure 6 illustrates a combination of the averaged OH-PLIF flame and the corresponding centerline of the vortex structures at 85 Hz excitation and $Re = 5865$. The shear-layer/vortex centerline was estimated from both the Rayleigh images and the previously mentioned PIV results, and the Rayleigh values along this line were then manually extracted and curve fit. The centerline of the vortices lies between the flame (hot products) and the surrounding coflow. Based on the flame response, it seems clear that the differences in flow density, velocity, and temperature create an interface (shear layer) that is in a regime where it is susceptible to perturbations.

The influence of the acoustics and vortices on combustion has been previously investigated for a range of scenarios. Examining this as a driving mechanism for combustion instability [1], the general conclusion was that the frequency of vortex roll up can lock onto the frequency of a sound field if the amplitude of the acoustic oscillation is large enough and its frequency is sufficiently close to the natural frequency of vortex shedding. Lock-on phenomena was observed for Strouhal number on the order of unity, such as $St = 0.1$–0.2 for a premixed propane air flame in a side-dump combustor [5] and $St = 0.58$ for a premixed swirl-stabilized flame [25].

The conditions when the coupling occurred in this work are summarized in Fig. 7. The Strouhal number, $St_D = fD/U$, is based on the diameter of the burner and the mean velocity at the burner exit. Three conditions were tested, $Re = 5865$ and $\Phi = 0.51$, $Re = 6636$ and $\Phi = 0.63$, and $Re = 8547$ and $\Phi = 0.60$. Equivalence ratio did not show an impact on the coupling from 0.5 to 0.75 in the work of Kang et al. [17]. However, this work shows that the Reynolds number affects the range when the large-scale structures appear. When $Re = 5865$, the coupling occurs from 55 to 120 Hz, while the corresponding Strouhal number ranges from 0.27 to 0.87. When the Reynolds number is 8547, the coupling started when the excitation is

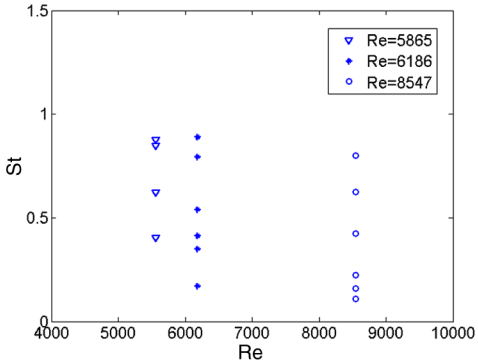

Fig. 7 Summary of unstable conditions.

22 Hz with $St_D = 0.11$. Based on the work of Kang et al. [17], the coupling occurred from $St_D = 0.17$ to 0.89 (frequency from 27 to 140 Hz) and with $Re = 6186$.

There has been much work on the instability of combustion [26–28]. As reviewed, acoustic excitation may induce three motions of a freejet, a convective motion, an acoustic propagation zone, and a mixed zone of the first two modes [15]. These modes are governed by St_D and St_θ (the shear-layer Strouhal number). It is generally agreed that the most amplified jet mode is $St_D = 0.4$, and the cutoff mode is $St_D = 1$; the most amplified shear-layer mode is $St_\theta = 0.032$, and the cutoff mode is $St_\theta = 0.08$. However, the range among the modes varies in different systems and is subject to change with different initial conditions [28]. The shear-layer Strouhal number of the experiments in this work is presented in Table 2, based on the flowfield measurement and the flowfield similarity of the LSB [24]. In general, the acoustic excitation in this work has St_D on the order of unity, and the conditions when the large-scale structure observed corresponds to St_D is less than one.

Figure 8 is the Rayleigh index value along the structure at 85 and 116 Hz excitation in Fig. 4. The Rayleigh index along the vortex line appears as a damping sinusoidal function. For the 85 Hz case, it can be fit with a sine function yielding a wave number $k = 218$ (damping is not considered in this calculation). From this wave number, a convective velocity is calculated as

$$v = 2\pi f/k = 2.43 \text{ m/s}$$

Similarly, the wave numbers and calculated velocities for other frequencies, when the shear layer and the acoustic excitation are coupled, are summarized in Fig. 9. It shows that the convective velocity stays relatively constant at about 70% of the mean velocity at the burner exit. This proves that the toroidal structures move with the mean flowfield but that they are frequency locked onto the frequency of the sound field. This wave number estimation was also carried out by Kang et al. [17] with similar results. The wave number there increased linearly with frequencies up to 125 Hz.

B. Phase-Resolved Variations

Rayleigh index and OH intensity distribution evolution during an acoustic cycle are shown in Figs. 10 and 11. One cycle is split into 36 phase segments, with segment 1 averaging data from 1–10 deg of phase, segment 2 covering 11–20 deg, and so on. Images are taken at different cycles and then resorted according to the gate signal of the camera and the pressure signal. Figure 10 illustrates a typical excitation at 116 Hz when a clear structure in the Rayleigh index was observed. For comparison, both the Rayleigh index and the OH intensity are normalized by their respective oscillation amplitude

Table 2 Shear-layer Strouhal number

	$Re = 5865$			$Re = 8547$		
f, Hz	13	100	208	22	125	270
St_θ	0.015	0.115	0.239	0.017	0.098	0.213

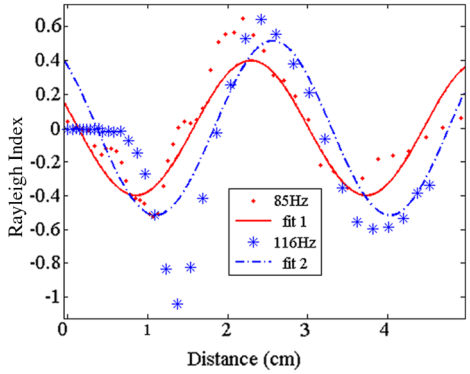

Fig. 8 Rayleigh index along the centerline of the vortex ring ($f = 85$, 116 Hz; $Re = 5865$, $\Phi = 0.51$).

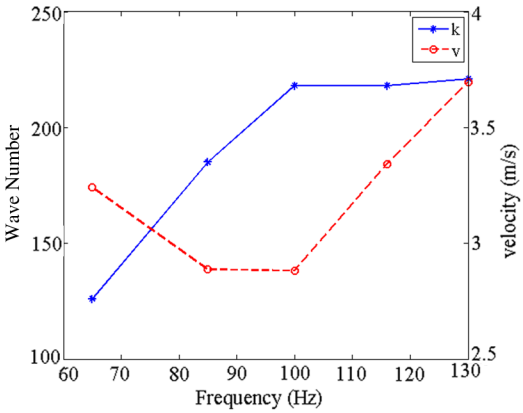

Fig. 9 Wave number and convective velocity ($Re = 5865$, $\Phi = 0.51$).

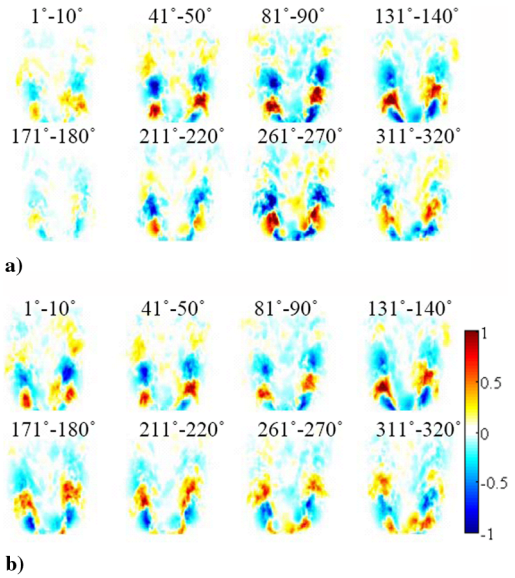

Fig. 10 Phase-resolved Rayleigh index and OH distribution at 116 Hz: a) Rayleigh index, b). OH intensity.

over a cycle. Figure 10a shows the Rayleigh index, and Fig. 11b the OH intensity for acoustic forcing at 116 Hz. The Rayleigh index map in each phase appears the same as the mean map over a cycle, but the phase-resolved OH-PLIF maps clearly capture the vortex evolution. The vortices are created at the exit plane and then convected while burning. Figure 11 illustrates excitation at 208 Hz. Because the acoustic field and the shear layer are not coupled at this frequency, there is no clear structure in the Rayleigh index or OH intensity maps.

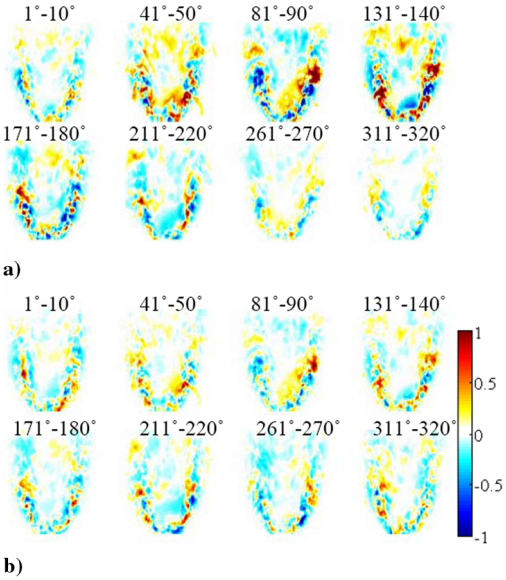

Fig. 11 Phase-resolved Rayleigh index and OH distribution at 208 Hz: a) Rayleigh index, b). OH intensity.

Phase-resolved analysis provides a vivid explanation about the positive–negative structure in Rayleigh index maps. When acoustic perturbation is enforced, the flow layer between the hot products and the surrounding cold flow becomes unstable and vortex structures are generated. The OH radical marks the underlying flowfield and is captured by the fluorescence signals. Because mass is conserved, the overall OH variation in a cycle should be zero. This also explains why the global Rayleigh index is close to zero. At each instant in time, the spatially averaged overall OH fluctuation is zero. As the pressure is assumed uniform across the whole field, the summation of the product of these two is also zero.

Figure 12 shows the pressure oscillation and global heat release (total OH intensity in the flame region) oscillation in one cycle at different frequencies. The dots represent experimental data and the smooth lines are from the curve fit. At 85 and 116 Hz, the heat release appears to respond directly to the acoustic excitation, whereas at 22 and 130 Hz, the heat release is quite chaotic. Apparently, the phase difference between the pressure and heat release is different at different frequencies. The phase difference changes with frequency if the structure is convected by the flowfield. Quantitative correlation of this coupling could contribute to improved analytical models for prediction and control of the instability. That will be an important aspect of this research effort.

C. Flame Surface Density

The main remaining question is whether Rayleigh index variation is induced by combustion intensity changes, flame surface density (FSD) changes, or some combination of both. This requires calculating the FSD, which here is approximated as FSD = total flame length/block area, and then comparing it to the total OH intensity within the area of interest. Detecting flame surface with OH-PLIF images has been applied in several studies [18–21]. In this work, the edge detection was performed with the MATLAB Canny Edge Detector. Figure 13 shows that the detection is quite accurate and sufficient for this analysis.

The flame surface detection and calculations are performed for each 10 deg of phase and then the results are normalized by their respective means to show the variation within the cycle. Figure 14a shows the regions of interest, which are selected according to strong Rayleigh index response. Figures 14b–14d are the graphs for area 1, 2, and 3, respectively. Results show good correlation between the flame surface density and OH intensity. The correlation coefficients between these two parameters are 0.90, 0.96, and 0.92 for the three blocks, respectively. It is clear that OH variation follows the FSD

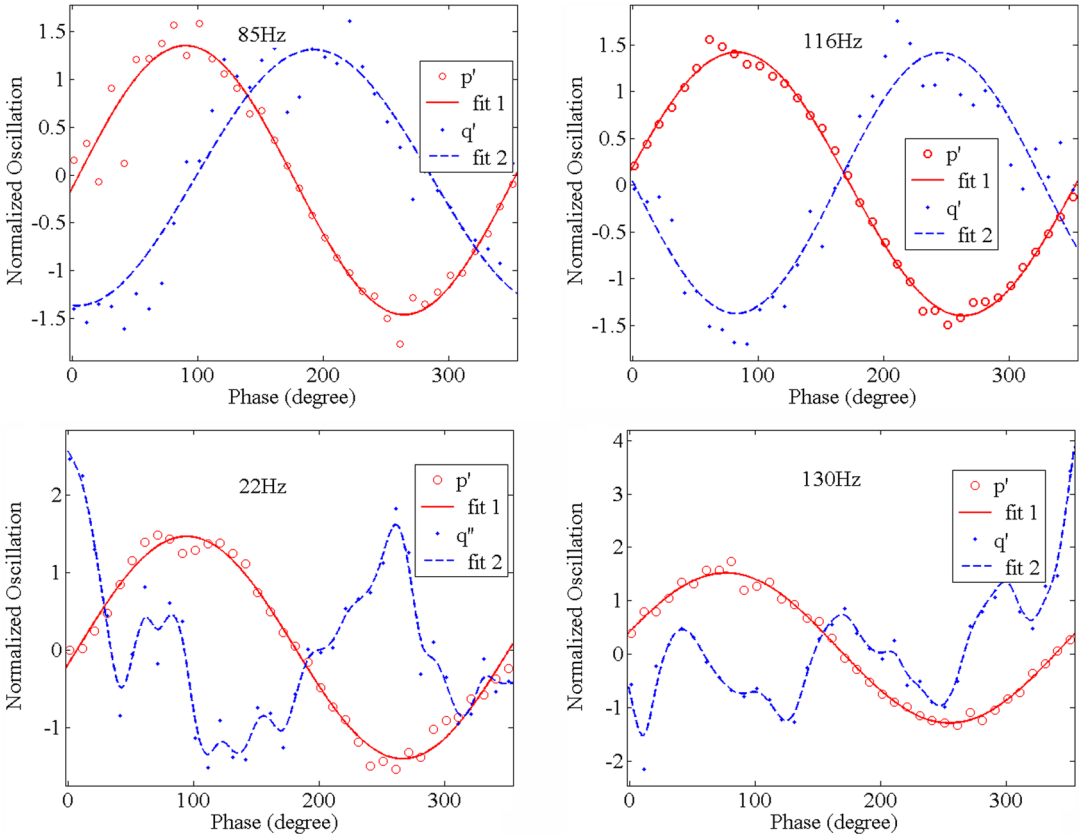

Fig. 12 Pressure and heat release oscillation at different frequencies.

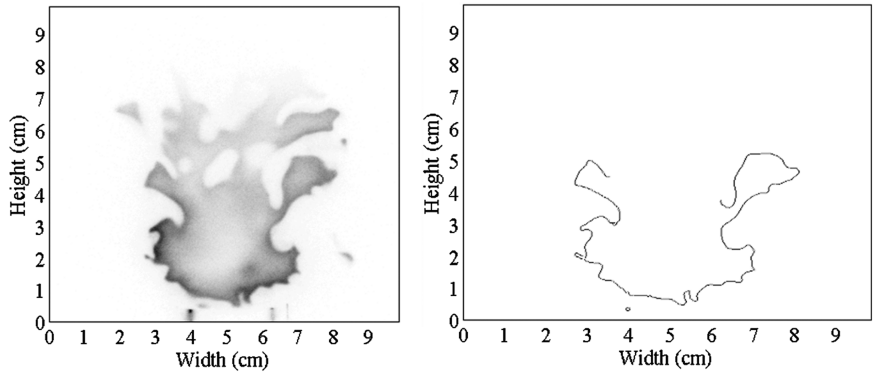

Fig. 13 Flame surface detection with MATLAB.

variation in a period, which implies that the OH intensity variation is caused by the distortion of flame surface rather than through local intensity changes. As an explanation of this periodic FSD variation in the shear layer, it seems clear that acoustic-flow coupling causes the neutrally stable shear layer to produces strong vortices at the acoustic forcing frequency. These vortices then deform the flame and create zones of high FSD between them (as the vortices roll up reactants ahead of the flame) and low FSD next to them (as the vortices pass and strain the flame into more of a flat surface). This variation in flame surface causes a net change in reactant consumption and a similar variation in the resulting heat release. This whole process transforms the coupling (phase locked) between the acoustic oscillation and the fluid mechanics into a heat release variation that induces the structures seen in the Rayleigh index. This is different from other systems where flame vortex interaction has been studied and mathematical models constructed for predicting the flame response. The existing models fall into several categories: laminar flame disturbed by a vortex, anchored (and nonwrinkled) turbulent flames [16], and mildly turbulent flames that are engulfed and rolled into large vortices [18]. The behavior encountered here with the LSB involves a highly wrinkled flame surface (as is evident from Fig. 3a) that is compacted or elongated, depending on location, by the passage of vortices. The resulting change in local FSD is approximately a 30% increase in front of the vortex and a 30% decrease as the vortex passes by, with the total FSD remaining unchanged. This is again very different from configurations where the flame surface is initially smooth and the vortex passage creates a smooth curve deformation. Also, the other studies all involve local acoustic driving which creates a companion mass flow oscillation that would induce a variation in the total FSD.

The FSD analysis also shows, as expected, that products zones that have slowly varying OH concentrations are filtered out by the analysis process and do not significantly contribute to the resulting data. This validates the methodology and indicates its broad applicability for providing significant insight into a range of turbulent or fluctuating flames.

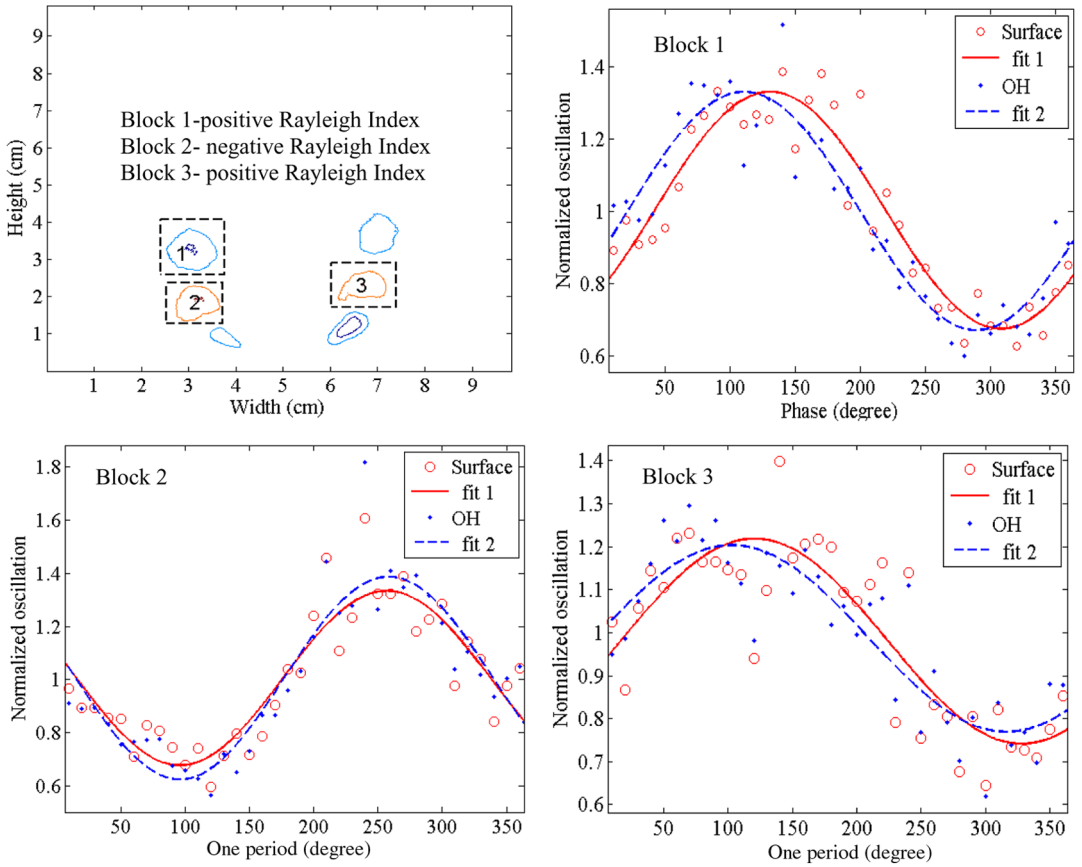

Fig. 14 Local FSD and OH intensity variation over a cycle ($\Phi = 0.5, P = 1$ bar, $f = 116$ Hz).

IV. Conclusions

The goal of this study was to explain the previously reported toroidal structure in the Rayleigh index maps for certain cases of acoustic forcing with the low-swirl burner. What has been found is that the acoustic perturbation couples to the shear-layer vortex generation mechanism. To further investigate this phenomenon, the stability was examined at different flow conditions with $Re = 5865$–8547. The span of frequency, across which phase locking occurred, changes with the Reynolds number and appears broader at high Reynolds number. In general, the corresponding jet Strouhal numbers are on the order of unity when the coupling occurs. A flame surface density analysis shows a close correlation between the FSD and the local OH intensity graphs. This indicates that the changes in flame heat release are driven by changes in the amount of flame surface rather than flame intensity. This supports the argument that the flame is deformed due to flow structures rather than intensified by local velocity oscillations (and the induced flame strain effects). With collection of data at additional experimental conditions, it is expected that a model capable of predicting the change in FSD will be formulated.

More broadly, this is the first time a system has been characterized in detail where extremely weak forcing is able to trigger a neutrally stable flow system into producing strong, large-scale structures that then have a clear impact on flame stability. Many previous studies have shown that strong forcing easily produces this type of result and that weak forcing can trigger flow changes, but this is the first clear characterization of a system where weak forcing (typical of gas turbine ambient conditions) can induce the observed strong flame oscillations. The implication of this work is that there can be other neutrally stable flowfields that will undergo drastic changes due to the presence of flame-induced ambient noise. These can give rise to combustion instabilities that cannot be predicted by existing theory or with current computer models. To further explain and characterize these effects is the goal of our continuing work.

Acknowledgments

The authors would like to thank R. K. Cheng for providing the burner, D. M. Kang for helping with the system configuration and experiment during his visit at the University of Iowa, and graduate students Hui Gao and Brett Bathel for help with the experiment. The authors would also like to thank Lawrence Berkeley National Lab (R. K. Cheng, project monitor), Siemens (Scott Martin, project monitor), and the University of Iowa for financial support.

References

[1] Keller, J. J., "On the Interpretation of Vortex Breakdown," *AIAA Journal*, Vol. 33, No. 12, 1995, pp. 2280–2287. doi:10.2514/3.12980

[2] Dowling, A. P., and Morgans, A. S., "Feedback Control of Combustion Oscillations," *Annual Review of Fluid Mechanics*, Vol. 37, Jan. 2005, pp. 151–182. doi:10.1146/annurev.fluid.36.050802.122038

[3] Cheng, R. K., Yegian, D. T., Miyasato, M. M., Samuelsen, G. S., Benson, C. E., Pellizzari, R., and Loftus, P., "Scaling and Development of Low-Swirl Burners for Low Emission Furnaces and Boilers," *Proceedings of the Twenty-Eighth Symposium on Combustion*, Combustion Inst., Pittsburgh, PA, 2000, pp. 1305–1313.

[4] Lieuwen, T. C., and Yang, V. (eds.), "Combustion Instabilities in Gas Turbine Engines: Operational Experience, Fundamental Mechanisms, and Modeling," AIAA Progress in Astronautics and Aeronautics, Vol. 210, AIAA, Reston, VA, 2005, p. 657.

[5] Samaniego, J. M., Yip, B., Poinsot, T., and Candel, S., "Low-Frequency Combustion Instability Mechanisms in a Side-Dump Combustor," *Combustion and Flame*, Vol. 94, No. 4, 1993, pp. 363–380. doi:10.1016/0010-2180(93)90120-R

[6] Culick, F. E. C., "Nonlinear Behavior of Acoustic Waves in Combustion Chambers I," *Acta Astronautica*, Vol. 3, Nos. 9–10, 1976, pp. 735–757. doi:10.1016/0094-5765(76)90108-9

[7] Lieuwen, T., "Modeling Premixed Combustion-Acoustic Wave Interactions: A Review," *Journal of Propulsion and Power*, Vol. 19, No. 5, 2003, pp. 765–781. doi:10.2514/2.6193

[8] Giezendanner, R., Keck, O., Weigand, P., Meier, W., Meier, U., Stricker, W., and Aigner, M., "Periodic Combustion Instabilities in a Swirl Burner Studied by Phase-Locked Planar Laser Induced Fluorescence," *Combustion Science and Technology*, Vol. 175, No. 4, 2003, pp. 721–741. doi:10.1080/00102200302390

[9] Gutmark, E., Parr, T. P., Parr, D. M., and Schadow, K. C., "Planar Imaging of Vortex Dynamics in Flames," *Journal of Heat Transfer*, Vol. 111, No. 1, 1989, pp. 148–155.

[10] Ghoniem, A. F., Annaswamy, A., Wee, D., Yi, T., and Park, S., "Shear Flow Driven Combustion Instability Evidence Simulation and Modeling," *Proceedings of the Combustion Institute*, Combustion Inst., Pittsburgh, PA, 2002, pp. 53–60.

[11] Matveev, K. I., and Culick, F. E. C., "A Model for Combustion Instability Involving Vortex Shedding," *Combustion Science and Technology*, Vol. 175, No. 6, 2003, pp. 1059–1083. doi:10.1080/00102200302349

[12] Venkataraman, K. K., Preston, L. H., Simons, D. W., Lee, B. J., Lee, J. G., and Santavicca, D. A., "Mechanism of Combustion Instability in a Lean Premixed Dump Combustor," *Journal of Propulsion and Power*, Vol. 15, No. 6, 1999, pp. 909–917. doi:10.2514/2.5515

[13] Birbaud, A. L., Durox, D., and Candel, S., "Upstream Flow Dynamics of a Laminar Premixed Conical Flame Submitted to Acoustic Modulations," *Combustion and Flame*, Vol. 146, No. 3, 2006, pp. 541–552. doi:10.1016/j.combustflame.2006.05.001

[14] Huang, Y., Wang, S. W., and Yang, V., "A Systematic Analysis of Combustion Dynamics in a Lean-Premixed Swirl-Stabilized Combustor," *AIAA Journal*, Vol. 44, No. 4, 2006, pp. 724–740. doi:10.2514/1.15382

[15] Birbaud, A. L., Durox, D., Ducruix, S., and Candel, S., "Dynamics of Free Jets Submitted to Upstream Acoustic Modulations," *Physics of Fluids*, Vol. 19, No. 1, 2007, p. 013602. doi:10.1063/1.2432156

[16] Birbaud, A. L., Durox, D., Ducruix, S., and Candel, S., "Dynamics of Confined Premixed Flames Submitted to Upstream Acoustic Modulations," *Proceedings of the Combustion Institute*, Vol. 31, No. 1, 2007, 1257–1265. doi:10.1016/j.proci.2006.07.122

[17] Kang, D. M., Culick, F. E. C., and Ratner, A., "Combustion Dynamics of a Low-Swirl Combustor," *Combustion and Flame*, Vol. 151, No. 3, 2007, pp. 412–425. doi:10.1016/j.combustflame.2007.07.017

[18] Balachandran, R., Ayoola, B. O., Kaminski, C. F., Dowling, A. P., and Mastorakos, E., "Experimental Investigation of the Nonlinear Response of Turbulent Premixed Flames to Imposed Inlet Velocity Oscillations," *Combustion and Flame*, Vol. 143, Nos. 1–2, 2005, pp. 37–55. doi:10.1016/j.combustflame.2005.04.009

[19] Ayoola, B. O., Balachandran, R., Frank, J. H., Mastorakos, E., and Kaminski, C. F., "Spatially Resolved Heat Release Rate Measurements in Turbulent Premixed Flames," *Combustion and Flame*, Vol. 144, Nos. 1–2, 2006, pp. 1–16. doi:10.1016/j.combustflame.2005.06.005

[20] Cattolica, R. J., "OH Radical Nonequilibrium in Methane-Air Flat Flames," *Combustion and Flame*, Vol. 44, Nos. 1–3, 1982, pp. 43–59. doi:10.1016/0010-2180(82)90062-1

[21] Roberts, W. L., Driscoll, J. F., Drake, M. C., and Goss, L. P., "Images of Quenching of a Flame by a Vortex-To Quantity Regimes of Turbulent Combustion," *Combustion and Flame*, Vol. 94, Nos. 1–2, 1993, pp. 58–69. doi:10.1016/0010-2180(93)90019-Y

[22] Swift, G. W., "*Thermoacoustics: A Unifying Perspective for Some Engines and Refrigerators*," Acoustical Society of America, Sewickley, PA, 2002

[23] Lieuwen, T., and Cho, J. H., "Coherent Acoustic Wave Amplification/Damping by Wrinkled Flames," *Journal of Sound and Vibration*, Vol. 279, Nos. 3–5, 2005, pp. 669–686. doi:10.1016/j.jsv.2003.11.050

[24] Littlejohn, D., and Cheng, R. K., "Fuel Effects on a Low-Swirl Injector for Lean Premixed Gas Turbines," *Proceedings of the Combustion Institute*, Vol. 31, No. 2, 2007, pp. 3155–3162. doi:10.1016/j.proci.2006.07.146

[25] Paschereit, C. O., Gutmark, E., and Weisensenstein, W., "Coherent Structures in Swirling Flows and Their Role in Acoustic Combustion Control," *Physics of Fluids*, Vol. 11, No. 9, 1999, pp. 2667–2678. doi:10.1063/1.870128

[26] Coats, C. M., "Coherent Structures in Combustion," *Progress in Energy and Combustion Science*, Vol. 22, No. 5, 1996, pp. 427–509. doi:10.1016/S0360-1285(96)00011-1

[27] Huerre, P., and Monkewitz, P. A., "Local and Global Instabilities in Spatially Developing Flows," *Annual Review of Fluid Mechanics*, Vol. 22, Jan. 1990, pp. 473–537. doi:10.1146/annurev.fl.22.010190.002353

[28] Gutmark, E. L., and Ho, C.-M., "Preferred Modes and the Spreading Rates of Jets," *Physics of Fluids*, Vol. 26, No. 10, 1983, pp. 2932–2938. doi:10.1063/1.864058

T. Lieuwen
Associate Editor